## Journal of
## Applied and Computational Mechanics

Shahid Chamran
University of Ahvaz

**Research Paper**

# A Modified Couple Stress-Based Model for the Nonlinear Vibrational Analysis of Nano-Disks Using Multiple Scales Method

Ali Alizadeh[1], Mohammad Shishesaz[2], Shahram Shahrooi[3], Arash Reza[4]

[1] Department of Mechanical Engineering, Ahvaz Branch, Islamic Azad University, Ahvaz, Iran, Email: ali-alizadeh@iauahvaz.ac.ir

[2] Department of Mechanical Engineering, Shahid Chamran University of Ahvaz, Ahvaz, Iran, Email: mshishehsaz@scu.ac.ir

[3] Department of Mechanical Engineering, Ahvaz Branch, Islamic Azad University, Ahvaz, Iran, Email: shahramshahrooi@iauahvaz.ac.ir

[4] Department of Mechanical Engineering, Ahvaz Branch, Islamic Azad University, Ahvaz, Iran, Email: a.reza@iauahvaz.ac.ir

**Abstract:** In this article, the nonlinear vibrational behavior of a nano-disk was analyzed using the multiple scales method (MSM). The modified couple stress theory was used to consider the small-scale effect via the application of nonlocal parameter. Employing Hamilton's principle, two coupled nonlinear differential equations were derived based on the nonlinear von-Kármán strain-displacement relation and the classical plate theory. The Galerkin-based procedure was utilized to obtain a Duffing-type nonlinear ordinary differential equation with a cubic nonlinear term and solved by the application of MSM. The effects of nonlocal parameter, aspect ratio, different boundary conditions, and the nonlinear shift frequencies, were obtained on the overall behavior of the nano-disk. Results indicate that increasing the central dimensionless amplitude of the nano-disk, the nonlinear frequency, and the shift index exhibit an increasing behavior, while the increase in the non-dimensional nonlocal parameter, causes a decrease in the nonlinear frequency ratios and the shift index. Additionally, the increase in $h/r$ increases the effect of dimensionless central amplitude on the nonlinear frequencies ratios. Additionally, comparison of the current results with those previously published in the literature shows good agreements. This indicates that the MSM can ease up the solution, and hence, can be applied to the solution of nonlinear nano-disks with high accuracy.

**Keywords:** Multiple scales method; modified couple stress theory; nano-disk; nonlinear vibration.

## 1. Introduction

Nanotechnology is defined as designing, characterizing, producing, and applying structures, devices, and systems by controlling shape and size at the nanoscale. It utilizes all the conventional scientific and engineering subjects to accomplish novel applications using phenomena where small size is the best way to achieve a helpful property. The physicist Richard Feynman first put it forward.

One of the well-known and widely utilized nanostructures in the industry is nano-disk, especially those in micron and sub-micron sizes, which are of practical concern in several NEMS devices, including oscillators, clocks, sensors micro-gyroscopes (Tsai et al., [1]; Tsai et al., [2]; Tsai et al., [3]), and micro-motors (Lee et al., [4]). One of the essential photonic devices is a nanoscale refractive index sensor with a nano-disk resonator, which is frequently utilized in biosensors (Dolatabady et al., [5]). Besides, several attempts have been performed to monitor the biological behavior of nanoparticles. In this regard, many studies have been conducted on safer imaging agents for biomedical applications (Zhang et al., [6]), focusing on nano-disks and nano-spheres. Furthermore, micro/nano-disks are widely utilized in resistive switching phenomena (Hwang et al., [7]), cell structures (Horejs et al., [8]), solar cells (Hägglund et al., [9]; Huang et al., [10]), nano-disk array electrodes (Ito et al., [11]; Ito and Perera, [12]; Luo and White, [13], lasers (Chin et al., [14]; Cao et al., [15]; Van Campenhout et al., [16]; Kwon et al., [17]), and sensors (Cho and Jokerst, [18]).

Three experimental, molecular dynamics simulations and continuous environment theory methods are utilized to investigate nanostructure behavior because of their small size. Experimental methods in the nanoscale are very costly and challenging to execute. The molecular dynamics (MD) simulation is time-consuming and incapable of dealing with large-size nanostructures because it is restricted to structures with fewer molecules and atoms. Accordingly, utilizing several continuum theories have been suggested in the last decade owing to the fact that the classical continuum theories cannot predict the small-scale effect. Therefore, many higher-order theories have been developed to predict the size effect in the nanostructures, including the strain gradient theory, (Aifantis, [19]; Anjomshoa and Tahani, [20]; Sedighi, [21]; Koochi, [22]), Mindlin's strain gradient theory (Mindlin

and Eshel, [23]), couple stress theory (Toupin, [24]), modified couple stress theory (Yang et al., [25]), nonlocal elasticity theories (Eringen, [26]; Eringen, [27]; Eringen, [28]; shishesaz et al., [29]; shishesaz et al.,[30]; Barretta et al., [31]; Demir et al., [32]; Malikan [33]) peri dynamic theory (Chen et al., [34]; Diyaroglu et al., [35]; O'Grady and Foster, [36]); stress-driven nonlocal theory (Barretta et al., [37]; Barretta et al., [38]; Barretta et al., [39]).

For example, in the study by (Romano et al. [40]), the nonlocal elasticity was addressed in the context of geometrically linearized structural models. Two iterative solution methods for the stress-driven and mixture strain-driven models were introduced. The iterative procedure for the stress-driven models yields the exact solution just at the first step of the iteration. The iterative solution relevant to the mixture strain-driven models do not exhibit such property, yet, convergence is always asymptotic and fast. Apuzzo et al. (Apuzzo et al., [41]) analyzed the axial and torsional free vibrations of elastic nano-beams by stress-driven two-phase elasticity.

The modified couple stress theory has been frequently utilized to analyze the size-dependent mechanical responses of micro/nanostructures with reasonable accuracy. Based on the results, the theory is consistent with the experimental results than the Eringen's nonlocal elasticity (Miandoab et al., [42]), where, unlike the classical couple stress theory, the couple stress tensor includes one material length scale parameter related to the symmetric rotation gradient tensor.

So far, this theory has been utilized to investigate the static and dynamic behaviors of nanostructures. For example, (Asghari et al., [43]) have studied the size-dependent Timoshenko beams based on the couple stress theory. The thermoelastic behavior of nano-sized film/substrate multilayers with poor interfaces and size-dependent characteristics has also been studied using this theory (Liu and Chen, [44]). In a study by Baghani (Baghani, [45]), the length scale parameter of silicon has been identified by fitting the pull-in voltage of several micro-beams utilizing modified couple stress theory. In a study by Akgöz and Civalek (Akgöz and Civalek, [46]), thermo-mechanical size-dependent buckling of embedded functionally graded (FG) microbeams has been examined using the sinusoidal shear deformation beam and modified couple stress theories. Pal and Das (Pal and Das, [47]) formulated the motion equation and boundary conditions for a rotary functionally graded annular microsystem through modified couple stress theory, Kirchhoff theory, and Hamilton's principle. In the study by Shaat et al. (Shaat et al., [48]), the size-dependent bending of Kirchhoff nano-plates has been analyzed using a modified couple stress theory. Besides, 'micro shells' dynamic and stability behaviors have been analyzed using a modified couple stress theory and different shell theories. (Veysi et al., [49]; Jouneghani et al., [50]).

The modified couple stress theory has been applied in several works to study vibration in nanostructures, including nanotubes, nano-beams, nano-plates, and nano-shells. For example, the nonlinear dynamics of circular microplates were analyzed asymmetrically by Wang et al. (Wang et al., [51]). Karamanli (Karamanli and Aydogdu, [52]) has studied the vibration information of a laminated micro-beam concerning the effects of physical parameters on structural stability. Ghadiri and Shafiei (Ghadiri and Shafiei, [53]) have analyzed the vibration in rotating functionally graded Timoshenko micro-beam, utilizing the modified couple stress theory under different temperature distributions. Ghadiri and SafarPour (Ghadiri and SafarPour, [54]) analyzed the free vibration characteristics of functionally graded porous micro-shell in the thermal environment using the first-order shear model and modified couple stress theory. Malikan et al. (Malikan et al., [55]) analyzed Buckling of a Micro Composite Plate with Nano Coating Based on the Modified Couple Stress Theory. Consequently, the modified couple stress theory is of great importance in qualifying the mechanical responses of small-scale structures.

Natural frequencies and other nonlinear dynamic properties play an essential role in designing and analyzing different nanostructures like nano-plates, nano-beams, and nano-shells. For this, wide research attention has been paid to the nonlinear analysis of nanostructures in recent years. For example, the nonlinear free vibration of isotropic single-layer nano-plates was analyzed by (Jomehzadeh and Saidi, [56]) utilizing nonlocal elasticity theory. The nonlinear forced vibration of isotropic and classical nano-plates, which were based on simple supports and followed the theory of nonlocal elasticity, was studied by He et al. (He et al., [57]). In the study performed by Zhang et al. (Zhang et al., [58]), the nonlinear vibrations of rectangular graphene nano-sheet were investigated

It isn't easy to find an exact solution to the nonlinear vibration in nanostructures, so it is possible to use an approximate analytical approach or numerical technique to this end. The multiple-scale method (MSM), as a powerful and efficient analytical technique, has been applied to engineering dynamics problems and to study the vibration in nanostructures, to solve highly nonlinear problems, for example, Foda (Foda, [59]) utilized MSM to analyze the nonlinear vibrations in a beam having pinned ends concerning the effects of shear deformation and rotary inertia. Ramezani et al. (Ramezani et al., [60]) utilized the same method for the same problem based on the boundary conditions for a double clamped beam. They found that shear deformation and rotary inertia effects need to be considered for an accurate dynamic analysis when the beam theory is utilized to analyze the micro/nano-electromechanical structures. EL- dib et al. (El-Dib et al., [61]) analyzed Stability of a Strongly Displacement Time-Delayed Duffing Oscillator Using Multiple Scales Homotopy Perturbation Method.

The present study aims to study the nonlinear free vibrational behavior of a nano-disk. The differential equations are derived based on the modified couple stress theory and the Hamilton principle, while the inertial and shear stress effects were ignored. For this purpose, the equation of motion is discredited utilizing the Galerkin weighted residual method. The transverse displacement is expressed in terms of finite series of basic functions, namely the linear free vibrational mode shapes described in terms of Bessel's functions. The nonlinear time variable equations are eliminated utilizing the Galerkin method, and then, using MSM, the natural nonlinear frequencies are extracted. A comparison with the relevant literature confirms this approach's validity. The following sections in this study discuss the numerical results, including the effects of nonlocal parameters, aspect ratios, different boundary conditions, and nonlinear shift frequencies on the nano-disks' overall behavior. Finally, the results can function as a profound guiding foundation for designing nano-motors, nano-rotors, and other rotary nano-structures. In most studies, the nonlinear vibrations of the nano-structures, as well as the nonlinear natural frequencies have been studied only in one main mode due to the complexity of the calculations. In the present article, however, nonlinear frequencies are explored and analyzed in several modes using the unique method presented.

## 2. Modified Couple Stress Relations

The modified couple stress theory is one of the widely utilized size-dependent continuum theories proposed by Yang et al. (Yang et al., 2002 [25]). The classical couple stress theory contains two classical and two additional material constants for isotropic elastic materials. The two additional constants are related to the material's underlying nanostructure and are inherently difficult to determine. Yang proposed the modified couple stress theory involving only one additional material length scale parameter. This feature makes the modified couple stress theory easier to utilize. Based on this theory, the strain energy density is a function of both strain and gradient of rotation vector.

Based on this theory, the elastic potential energy is in the following form:

$$U = \frac{1}{2} \int_V (\sigma : \varepsilon + m : \delta\chi) dv \tag{1}$$

where the strain tensor $\varepsilon$ and the symmetric part of the curvature tensor $\chi$ can be written as;

$$\varepsilon = \frac{1}{2}\left[\nabla u + (\nabla u)^T\right] \tag{2}$$

$$\chi = \frac{1}{2}\left[\nabla\omega + (\nabla\omega)^T\right] \tag{3}$$

Here, $u$ is a displacement vector and $\omega$ is the rotation vector defined as:

$$\omega = \frac{1}{2}curl(u) \tag{4}$$

Two states of stress are described by the stress tensor $\sigma$, and the deviatoric part of the couple stress tensor $m$ is given as follows:

$$\sigma = \lambda tr(\varepsilon)\delta + 2\mu\varepsilon \tag{5}$$

$$m = 2l^2\mu\chi \tag{6}$$

In the above equations, $\lambda$ and $\mu$ are Lamé's constants, $l$ is the material length-scale parameter regarded as a material property characterizing the effect of couple stress.

This model has only one additional material length scale parameter and includes the symmetric couple stress, while in the formulations of modified strain gradient theory (Yang et al., 2002 [25]) there are three independent length scale parameters. Hence, modified couple stress theory is adopted in this research.

It is worth noting that the deformation measures describing the couple stress theory are kinematically redundant. Recently, researchers have considered this redundancy and proposed simple models which are free from the inherent conceptual weakness of most redundant models (Romano et al., [62]; Barbagallo et al., [63]; Neff et al., [64]).

## 3.   Problem Formulation

The derivation in this section is performed on an isotropic axisymmetric von Kármán circular plate. According to this theory, the straight lines initially normal to the mid surface remain straight and normal to that surface after bending. The stress normal to the mid-plane, $\sigma_z$, is small compared with the other stresses and may be neglected in stress-strain relations. Nonetheless, despite the small strains for the plate, the mid-plane rotations are moderate and may not be neglected.

For the axisymmetric vibration of a Kirchhoff nano-disk, the displacements $u_r$, $u_\theta$ and $u_z$ can be expressed in terms of the displacements of a point on the middle surface of the plate as:

$$
\begin{aligned}
u_r(r,\theta,z,t) &= u(r,\theta,t) - z\frac{\partial w}{\partial r}(r,\theta,t), \\
u_\theta(r,\theta,z,t) &= v(r,\theta,t) - z\frac{1}{r}\frac{\partial w}{\partial\theta}(r,\theta,t), \\
u_z(r,\theta,z,t) &= w(r,\theta,t)
\end{aligned}
\tag{7}
$$

where $r \in [0,R]$, and $u_r$, $u_\theta$ and $u_z$ are the radial, angular, and transverse displacements, respectively. Furthermore, $u$, $v$, and $w$ are the radial, angular, and transverse displacements of the plate mid surface, respectively.

According to the von Kármán plate theory, the nonzero nonlinear strain components for the large-amplitude vibrations of a circular plate takes the form of:

$$
\begin{aligned}
\varepsilon_{rr} &= \frac{\partial u_r}{\partial r} + \frac{1}{2}\left(\frac{\partial u_z}{\partial r}\right)^2 \\
\varepsilon_{\theta\theta} &= \frac{u_r}{r} + \frac{1}{r}\frac{\partial u_\theta}{\partial\theta} + \frac{1}{2}\left(\frac{1}{r}\frac{\partial u_z}{\partial\theta}\right)^2 \\
\gamma_{r\theta} &= \frac{1}{r}\left(\frac{\partial u_r}{\partial\theta} - u_\theta\right) + \frac{\partial u_\theta}{\partial r} + \frac{1}{r}\frac{\partial u_z}{\partial r}\frac{\partial u_z}{\partial\theta}
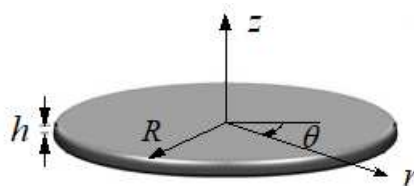\end{aligned}
\tag{8}
$$



**Fig. 1.** Geometry and coordinate system of the nano-disk.

Substituting the displacement components given in Eq. (7) back into Eq. (8) and realizing that for axisymmetric loading $\partial / \partial\theta = 0$, and $v = 0$, then, the first two expressions in Eq. (8) can be reduced into:

$$\varepsilon_{rr} = \frac{\partial u}{\partial r} + \frac{1}{2}\left(\frac{\partial w}{\partial r}\right)^2 - z\frac{\partial^2 w}{\partial r^2}$$
$$\varepsilon_{\theta\theta} = \frac{u}{r} - \frac{z}{r}\frac{\partial w}{\partial r}$$

(9)

The component of the rotation vector and the corresponding symmetric curvature tensor can be obtained from Eqs. (3) and (4) as:

$$\omega_1 = \frac{1}{r}\frac{\partial}{\partial\theta}w(r,\theta,t) \quad \omega_2 = -\frac{\partial}{\partial r}w(r,\theta,t)$$
$$\omega_3 = \frac{1}{2r}\left(v(r,\theta,t) - \frac{z\left(\frac{\partial}{\partial\theta}u(r,\theta,t)\right)}{r} + r\left(\frac{\partial}{\partial r}v(r,\theta,t) + \frac{z\left(\frac{\partial}{\partial\theta}u(r,\theta,t)\right)}{r^2} - \frac{z\left(\frac{\partial^2}{\partial\theta\partial r}w(r,\theta,t)\right)}{r}\right)\right)$$

(10)

Additionally, for axisymmetric vibrational analysis, Eq. (10) can be reduced into:

$$\omega_2 = -\frac{\partial}{\partial r}w(r,t)$$

(11)

The corresponding symmetric curvature tensor can be obtained from Eqs. (3) and (11) as follows:

$$\chi_{r\theta} = \frac{1}{2}\left(\frac{\partial\omega_1}{\partial\theta} + \frac{1}{r}\frac{\partial\omega_2}{\partial r}\right) = \frac{1}{2}\left(\frac{1}{r}\frac{\partial w(r,t)}{\partial r} - \frac{\partial^2 w(r,t)}{\partial r^2}\right)$$

(12)

Based on these equations, the governing equations of motion and the corresponding boundary conditions for a nano-disk can be obtained utilizing Hamilton's principle as:

$$\int_{t_1}^{t_2}[\delta T - \delta U + \delta W]dt = 0$$

(13)

where $U$, $W$ and $T$ are the strain energy, work of external loads, and kinetic energy of the nano-disk, respectively.

The first variation in the work done by the external forces in terms of transverse loading $p$, as well as the first variation in the kinetic energy of a structure, is given by:

$$\delta W = \int_{\Omega}[p\delta w]d\Omega$$
$$\delta T = \int_{\Omega}\left[I_0\left(\dot{u}\delta\dot{u} + \dot{w}\delta\dot{w}\right) + I_2\left(\frac{\partial\dot{w}}{\partial r}\frac{\partial\delta\dot{w}}{\partial r}\right) - I_1\left(\dot{u}\frac{\partial\delta\dot{w}}{\partial r} + \delta\dot{u}\frac{\partial\dot{w}}{\partial r}\right)\right]rdrd\theta$$

(14)

where, $I_1$, $I_2$ and $I_0$ are the longitudinal and rotary inertias, respectively. These parameters are defined as:

$$I_0 = \int_{-h/2}^{h/2}\rho dz = \rho h, \quad I_1 = 0, \quad I_2 = \int_{-h/2}^{h/2}\rho z^2 dz = \frac{1}{12}\rho h^3$$

(15)

Moreover, the variation in strain energy is given by:

$$\delta U = \int_{V}(\sigma.\delta\varepsilon + m.\delta\chi)dV$$

(16)

Following the appropriate replacement of the Lamé's constants by the modulus of elasticity $E$ and Poisson's ratio $v$, and the use of Eqs. (5) and (6), the stress and deviatoric parts of the couple stress tensor take the following form:

$$\sigma_{rr} = \frac{E_0}{(1-v^2)}\left[\frac{\partial u(r,t)}{\partial r} + \frac{1}{2}\left(\frac{\partial w(r,t)}{\partial r}\right)^2 - z\frac{\partial^2 w}{\partial r^2} + v\left(\frac{u(r,t)}{r} - \frac{z}{r}\frac{\partial w(r,t)}{\partial r}\right)\right]$$
$$\sigma_{\theta\theta} = \frac{E_0}{(1-v^2)}\left[\frac{u(r,t)}{r} - \frac{z}{r}\frac{\partial w(r,t)}{\partial r} + v\left(\frac{\partial u(r,t)}{\partial r} + \frac{1}{2}\left(\frac{\partial w(r,t)}{\partial r}\right)^2 - z\frac{\partial^2 w(r,t)}{\partial r^2}\right)\right]$$
$$\sigma_{r\theta} = 0$$

(17)

$$m_{r\theta} = 2l^2 G_0\chi_{r\theta} = l^2 G_0\left(\frac{1}{r}\frac{\partial w(r,t)}{\partial r} - \frac{\partial^2 w(r,t)}{\partial r^2}\right)$$

(18)

Substituting Eqs. (17) and (18) into Eq. (16) and integrating by parts and collecting the similar terms, can obtain the following result:

$$\delta U = \int_{\Omega} \left[ \delta u \left( (-N_r r)_{,r} + (N_\theta) \right) + \delta w \left( \left( -N_r r \frac{\partial w}{\partial r} \right)_{,r} + (-M_r r)_{,rr} + (M_\theta)_{,r} + \left( -\frac{1}{2} r R_{r\theta} \right)_{,rr} \right) \right] (dr d\theta) \qquad (19)$$

It is worth mentioning that the following stress resultants ($N_r$, $N_\theta$), moment resultants ($M_r$, $M_\theta$), as well as the couple resultants ($R_{r\theta}$) are defined as below:

$$(N_r, N_\theta) = \int_{-\frac{h}{2}}^{\frac{h}{2}} (\sigma_{rr}, \sigma_{\theta\theta}) dz$$

$$(M_r, M_\theta) = \int_{-\frac{h}{2}}^{\frac{h}{2}} z (\sigma_{rr}, \sigma_{\theta\theta}) dz \qquad (20)$$

$$R_{r\theta} = \int_{-\frac{h}{2}}^{\frac{h}{2}} m_{r\theta} dz$$

Substituting the expression for $\delta W, \delta T, \delta U$ from Eqs. (14) and (16) into Eq. (13) and integrating the terms while collecting the coefficients of $\delta u, \delta v, \delta w$ the equations of motion for the nano-disk are obtained as:

$$\delta u: \qquad \left[ r I_0 \ddot{u} \right] + \left( (-N_r r)_{,r} + (N_\theta) \right) = 0 \qquad (21)$$

$$\delta w: \qquad \frac{1}{r} \left( \left( +N_r r \frac{\partial w}{\partial r} \right)_{,r} + (r M_r)_{,rr} - (M_\theta)_{,r} + (r R_{r\theta})_{,rr} + (R_{r\theta})_{,r} \right) = \left( I_0 \ddot{w} - I_2 \frac{\partial^2}{\partial t^2} \left( \frac{1}{r} \left( \frac{\partial w}{\partial r} r \right)_{,r} \right) \right) \qquad (22)$$

The in-plane inertia term can be neglected for the cases in which the in-plane natural frequencies are significant compared with the natural transverse frequencies (Faris [65]), and then Eq. (21) may be written as:

$$\frac{\partial}{\partial r} (r N_r) - N_\theta = 0 \qquad (23)$$

Now, the stress function $F$ is referred to as the Airy stress function, is defined as (Shishesaz et al., [29]).

$$N_r = \frac{1}{r} \frac{\partial F}{\partial r} \quad , \quad N_\theta = \frac{\partial^2 F}{\partial r^2} \qquad (24)$$

As can be observed, this equation satisfies Eq. (23). Substituting Eq. (24) into Eq. (22), the equation of motion is obtained as:

$$\frac{1}{r} \left( \left( \frac{\partial F}{\partial r} \frac{\partial w}{\partial r} \right)_{,r} + (r M_r)_{,rr} - (M_\theta)_{,r} + (r R_{r\theta})_{,rr} + (R_{r\theta})_{,r} \right) = \left( I_0 \ddot{w} - I_2 \frac{\partial^2}{\partial t^2} \left( \frac{1}{r} \left( \frac{\partial w}{\partial r} r \right)_{,r} \right) \right) \qquad (25)$$

Additionally, the stress resultants can be expressed in terms of strains, as in Eqs. (26) and (27):

$$N_r = \frac{Eh}{1 - v^2} (\varepsilon_{rr} + v \varepsilon_{\theta\theta}) \qquad (26)$$

$$N_\theta = \frac{Eh}{1 - v^2} (v \varepsilon_{rr} + \varepsilon_{\theta\theta}) \qquad (27)$$

Then, on using Eqs. (8) and (9), Eqs. (28) and (29) can be recast as follows:

$$\left( \frac{1}{r} \frac{\partial F}{\partial r} \right) = \frac{Eh}{1 - v^2} \left[ \frac{\partial u}{\partial r} + \frac{1}{2} \left( \frac{\partial w}{\partial r} \right)^2 + v \frac{u}{r} \right] \qquad (28)$$

$$\frac{\partial^2 F}{\partial r^2} = \frac{Eh}{1 - v^2} \left\{ v \left( \frac{\partial u}{\partial r} + \frac{1}{2} \left( \frac{\partial w}{\partial r} \right)^2 \right) + \frac{u}{r} \right\} \qquad (29)$$

Eliminating $u$ from Eqs. (28) and (29), the compatibility equation is obtained as given in Eq. (30):

$$\left\{ r \frac{\partial^3 F}{\partial r^3} + \frac{\partial^2 F}{\partial r^2} - \frac{1}{r} \frac{\partial F}{\partial r} \right\} + \frac{1}{2} Eh \left( \frac{\partial w}{\partial r} \right)^2 = 0 \qquad (30)$$

Consequently, the equation of motion can be expressed in terms of displacement as:

$$(-D - A) [w_1(r,t)] + [L(F, w)] = \left( \rho h \ddot{w} - \frac{\rho h^3}{12} \frac{\partial^2}{\partial t^2} \left( \frac{1}{r} \left( \frac{\partial w}{\partial r} r \right)_{,r} \right) \right) \qquad (31)$$

where $D = h^3 E_0 / [12(1 - \nu^2)]$, $A = l^2 Gh$ and $G = E / [2(1 + v)]$, while $w_1(r,t)$ and $L(F, w)$ are expressed as:

$$w_1(r,t) = \nabla^4 w(t,r)$$
$$L(F,w) = \frac{1}{r}\left(F_{,r} w_{,r}\right)_{,r}$$

(32)

The differential operator $\nabla^4$ is given by:

$$\nabla^4 = \frac{\partial^4}{\partial r^4} + \frac{2}{r}\frac{\partial^3}{\partial r^3} - \frac{1}{r^2}\frac{\partial^2}{\partial r^2} + \frac{1}{r^3}\frac{\partial}{\partial r}$$

(33)

Equations (30) and (31) give the compatibility equation and equation of motion for the nonlinear vibration of a nano-disk, based on large deflections and modified couple stress theory. It is required that the corresponding solutions satisfy the related boundary conditions to determine the transverse displacement $w(r,t)$ and stress function $F(r,t)$. The boundary conditions for the simply supported and clamped edge constraints at $r = R$ are as follows:

simply supported:    $\dfrac{\partial F}{\partial r} = 0$  ,   $w(r,t) = 0$  ,   $M_{rr} = 0 @ \left(w_{,rr}(r,t) + v w_{,r}(r,t) = 0\right)$,

(34)

clamped edge:    $\dfrac{\partial^2 F}{\partial r^2} - \dfrac{v}{r}\dfrac{\partial F}{\partial r} = 0$  ,   $w(r,t) = 0$  ,   $\dfrac{\partial w(r,t)}{\partial r} = 0$,

(35)

For convenience, the following dimensionless variables and parameters are introduced into the solution:

$$w = h\bar{w},\ t = T\bar{t}\left(T = \sqrt{\frac{\rho h R^4}{D}}\right),\ r = R\bar{r},\ l = h l_0,\ \eta = \frac{h}{R},\ F = F^* \bar{F}\left(F^* = \frac{Eh^3}{2}\right)$$

(36)

On substituting Eq. (36) into Eqs. (30) and (31), the non-dimensional governing equations and the corresponding boundary conditions at $\bar{r} = 1$ are obtained as follows:

$$-(1+k_1)\left[\left(w_1(\bar{t},\bar{r})\right)\right] + k_2\left[L(\bar{F},\bar{w})\right] \equiv \ddot{\bar{w}} - \frac{\eta^2}{12}\frac{1}{\bar{r}}\frac{\partial^2}{\partial \bar{t}^2}\left(\frac{\partial \bar{w}}{\partial \bar{r}}\bar{r}\right)_{,\bar{r}}$$

$$k_1 = 6(1-v)\frac{l^2}{h^2},\ k_2 = 6\left(1-v^2\right),\quad L(\bar{F},\bar{w}) = \frac{1}{r}\left(\bar{F}_{,\bar{r}}\bar{w}_{,\bar{r}}\right)_{,\bar{r}}$$

(37)

$$\left\{\bar{r}\frac{\partial^3 \bar{F}}{\partial \bar{r}^3} + \frac{\partial^2 \bar{F}}{\partial \bar{r}^2} - \frac{1}{\bar{r}}\frac{\partial \bar{F}}{\partial \bar{r}}\right\} + \left(\frac{\partial \bar{w}}{\partial \bar{r}}\right)^2 = 0$$

(38)

Additionally, the boundary conditions at $\bar{r} = 1$ are obtained as follows:

simply supported:    $\dfrac{\partial \bar{F}}{\partial \bar{r}} = 0$  ,   $\bar{w}(\bar{r},\bar{t}) = 0$  ,   $M_{\bar{r}\bar{r}} = 0 @ \left(\bar{w}_{,\bar{r}\bar{r}}(\bar{r},\bar{t}) + v\bar{w}_{,r}(\bar{r},\bar{t}) = 0\right)$

(39)

clamped edge:    $\dfrac{\partial^2 \bar{F}}{\partial \bar{r}^2} - \dfrac{v}{\bar{r}}\dfrac{\partial \bar{F}}{\partial \bar{r}} = 0$  ,   $\bar{w}(\bar{r},\bar{t}) = 0$   ,   $\dfrac{\partial \bar{w}(\bar{r},\bar{t})}{\partial \bar{r}} = 0$

(40)

## 4.  Galerkin Weighted Residual Method

Equations (37)-(40) are the consistent basic equations for the nano-disk model. These equations that are the strong forms of the governing equations for the nano-disk based on nonlocal elasticity theory are reduced into equations of the classical circular plate provided l=0. Since finding the exact solution for the strong form of the nano-disk is commonly difficult, a weak form is usually generated for any further process. Here, as a general mathematical tool, the Galerkin weighted residual method is utilized to create the weak forms. According to this approach, the nonlinear free vibration response of the nano-disk can be obtained by introducing the following admissible function for the transverse deflection (Shishesaz et al., [29]):

$$w(\bar{r},\bar{t}) = \sum_{i=1}^{N} \varphi_i(\bar{r})q_i(\bar{t})\qquad,\qquad \bar{F}(\bar{r},\bar{t}) = \sum_{i=1}^{N} \psi_i(\bar{r})\tilde{q}_i(\bar{t})$$

(41)

In Eq. (41), N is the number of half-waves in the $r$ direction, $\varphi_i(\bar{r})$ are the known basic functions that should satisfy the boundary conditions of the nano-disk, and $q_i(\bar{t})$, $\tilde{q}_i(\bar{t})$ are the time variant-coefficient of the mode shape functions (Shishesaz et al., [29]) and $\psi_i(\bar{r})$ are obtained as follows (Shishesaz et al. [29]);

simply supprted :    $\psi_i(\bar{r}) = \varphi_i(\bar{r}) - \dfrac{1}{2}\bar{r}^2\varphi_i'(1)$,

clamped edge :    $\psi_i(\bar{r}) = \varphi_i(\bar{r}) - \dfrac{\bar{r}^2}{2(1-v)}\left\{\varphi_i''(1) - v\varphi_i'(1)\right\}$.

(42)

Using Eq. (41) in conjunction with the Galerkin method, Eq. (38) can be recast in the following form;

$$\int_0^1 \varphi_i.\bar{r}\left\{\sum_{r=1}^{N}\left\{\bar{r}\frac{d^3\psi_r}{d\bar{r}^3} + \frac{d^2\psi_r}{d\bar{r}^2} - \frac{1}{\bar{r}}\frac{d\psi_r}{d\bar{r}}\right\}\tilde{q}_i(\bar{t}) + \sum_{r=1}^{N}\left(\frac{d\varphi_r}{d\bar{r}}\right)q_r(\bar{t})\sum_{s=1}^{n}\left(\frac{d\varphi_s}{d\bar{r}}\right)q_s(\bar{t})\right\}d\bar{r} = 0\quad (i=1,...,n)$$

(43)

One can present the solution to Eq. (43) as;

$$\sum_{j=1}^{N} \alpha_{ij} \tilde{q}_j(\bar{t}) = \sum_{r=1}^{N} \sum_{s=1}^{N} \beta_{irs} q_r(\bar{t}) q_s(\bar{t}) \qquad (i = 1,...,n) \tag{44}$$

where,

$$\alpha_{ij} = \int_0^1 \varphi_i \left\{ \left\{ \bar{r} \frac{d^3 \psi_j}{d\bar{r}^3} + \frac{d^2 \psi_j}{d\bar{r}^2} - \frac{1}{\bar{r}} \frac{d\psi_j}{d\bar{r}} \right\} \right\} d\bar{r}, \tag{45}$$

$$\beta_{irs} = -\int_0^1 \varphi_i \left( \frac{d\varphi_r}{d\bar{r}} \right) \left( \frac{d\varphi_s}{d\bar{r}} \right) d\bar{r} \tag{46}$$

Solving Eq. (44) for the unknown mode shape functions $\tilde{q}_i(\bar{t})$, we obtain;

$$\tilde{q}_i(\bar{t}) = \sum_{j=1}^{N} \sum_{k=1}^{N} \gamma_{ijk} q_j(\bar{t}) q_k(\bar{t}) \qquad (i = 1,...,N) \tag{47}$$

Substituting Eq. (47) into Eq. (41) and applying the Galerkin method to the Eq. (37), the resulting equation can be recast in the following form:

$$\sum_{j=1}^{N} \left\{ M_{ij} \ddot{q}_j(\bar{t}) + K_{ij} q_j(\bar{t}) \right\} + \sum_{j=1}^{N} \sum_{k=1}^{N} \sum_{r=1}^{N} \sum_{s=1}^{N} G_{ijkrs} \, q_j(\bar{t}) q_r(\bar{t}) q_s(\bar{t}) = 0 \tag{48}$$

where $M_{ij}$ and $K_{ij}$ are the linear parameters and $G_{ijrsk}$ are the nonlinear parameters. These parameters are defined:

$$M_{ij} = \int_0^1 -\varphi_i(\bar{r}).\bar{r} \left[ \varphi_j(\bar{r}) - \frac{\eta^2}{12} \frac{1}{\bar{r}} \left( \frac{\partial \, \varphi_j(\bar{r})}{\partial \bar{r}} \bar{r} \right)_{,\bar{r}} \right] d\bar{r}$$

$$K_{ij} = \int_0^1 \varphi_i(\bar{r}).\bar{r} \left[ -(1 + k_1) \left[ \nabla^4 \varphi_j(\bar{r}) \right] \right] d\bar{r} \tag{49}$$

$$G_{ijrsk} = \int_0^1 \varphi_i(\bar{r}).\bar{r} \left[ k_2 \left[ \frac{1}{\bar{r}} \gamma_{jrs} \left( \psi_j(\bar{r})_{,\bar{r}} \varphi_k(\bar{r})_{,\bar{r}} \right)_{,\bar{r}} \right] \right] d\bar{r}$$

Equation (48) (Duffing equation) has received remarkable attention in recent decades due to a variety of engineering applications. Surveying the literature shows that different solution methods have been developed so far to solve this equation.

Based on Eq. (48), for the zero nonlinear parameters of $G_{ijrsk}$, the nonlinear Duffing equation has the following linear form:

$$\sum_{j=1}^{N} \left\{ M_{ij} \ddot{q}_j(\bar{t}) + K_{ij} q_j(\bar{t}) \right\} = 0 \tag{50}$$

The diagonalization procedure in linear algebra utilizes the modal matrix eigenvalues and eigenvectors. Accordingly, for decoupling Eq. (50), through this procedure, the following expression is introduced:

$$\{q_1, q_2,... q_N\}^T = \Phi \{p_1, p_2,... p_N\}^T \tag{51}$$

where $\Phi$ is a modal matrix for a linear system based on Eq. (50). On substituting Eq. (51) into Eq. (48) and multiply the result by the transposed matrix $\Phi^T$, Eq. (48) can be recast in the form of:

$$\bar{M}_{ii} \ddot{p}_i(\bar{t}) + \bar{K}_{ii} p_i(\bar{t}) + f_i(p_1,..., p_N) = 0 \tag{52}$$

where

$$\left[ \bar{M}_{ii} \right] = \Phi^T \left[ M_{ij} \right] \Phi$$

$$\left[ \bar{K}_{ii} \right] = \Phi^T \left[ K_{ij} \right] \Phi \tag{53}$$

$$f_i(p_1,..., p_N) = \sum_{j=1}^{n} \sum_{k=1}^{n} \sum_{r=1}^{n} \sum_{s=1}^{n} \Phi^T G_{ijkrs} \, \Phi^3 p_j(\bar{t}) p_r(\bar{t}) p_s(\bar{t})$$

Eq. (52) can be written in the form of:

$$\ddot{p}_i(\bar{t}) + \omega_{0,i}^2 p_i(\bar{t}) + \frac{1}{\bar{M}_{ii}} f_i(p_1,..., p_N) = 0 \tag{54}$$

where $\omega_{0,i}$ is defined as:

$$\omega_{0,i}^2 = \frac{\bar{K}_{ii}}{\bar{M}_{ii}} \tag{55}$$

Equation (55) is the linear natural frequency for linear vibration of the nano-disk.

## 5.  The Multiple Scales Method

The idea underlying MSM is that one can consider an expansion representing the response as a function of multiple independent variables, or scales, instead of one single variable. We begin by introducing novel independent variables according to (Nayfeh [66]).

$$T_n = \varepsilon^n t \quad n = 0, 1, 2, \ldots \tag{56}$$

Base on this method, the solutions to Eq. (54) can be expressed in the following form:

$$p_j(t,\varepsilon) = \varepsilon p_{0,j}(T_0, T_1, T_2) + \varepsilon^2 p_{1,j}(T_0, T_1, T_2) + \varepsilon^3 p_{2,j}(T_0, T_1, T_2) + \ldots \qquad (j = 1, \ldots, N) \tag{57}$$

where $T_0 = \bar{t}$ , $T_1 = \varepsilon \bar{t}$ , and $T_2 = \varepsilon^2 \bar{t}$ denote the fast and slow time scales. Introducing the partial differential operator's $D_r$ as:

$$D_r \equiv \frac{\partial}{\partial T_r}, r = 0.1, 2, \ldots \tag{58}$$

The first and second exact time derivatives are rewritten as follows:

$$\frac{d}{dt} = \frac{\partial}{\partial T_0} + \varepsilon \frac{\partial}{\partial T_1} + \varepsilon^2 \frac{\partial}{\partial T_2} + \ldots = D_0 + \varepsilon D_1 + \varepsilon^2 D_2 + \ldots,$$
$$\frac{d^2}{dt^2} = \frac{\partial}{\partial t}\left( \frac{\partial}{\partial T_0} + \varepsilon \frac{\partial}{\partial T_1} + \varepsilon^2 \frac{\partial}{\partial T_2} + \ldots \right) = D_0^2 + 2\varepsilon D_0 D_1 + \varepsilon^2 \left( D_1^2 + 2 D_0 D_2 \right) + \ldots \tag{59}$$

On substituting Eqs. (57) and (59) into Eq. (54), the approximate expressions for $\varepsilon^1, \varepsilon^2, \varepsilon^3$ can be derived as:

$$\varepsilon^1 : D^2_0 p_{0,j}(T_0, T_1, T_2) + \omega^2_{0,j} p_{0,j}(T_0, T_1, T_1) = 0 \tag{60}$$

Similarly,

$$\varepsilon^2 : D^2_0 p_{1,j}(T_0, T_1, T_1) + \omega^2_{0,j} p_{1,j}(T_0, T_1, T_1) = -2 D_0 D_1 p_{0,j}(T_0, T_1, T_2) \tag{61}$$

$$\varepsilon^3 : D^2_0 p_{2,j}(T_0, T_1, T_1) + \omega^2_{0,j} p_{2,j}(T_0, T_1, T_1) = -2 D_0 D_2 p_{0,j}(T_0, T_1, T_2) - D_1 D_1 p_{0,j}(T_0, T_1, T_2) - 2 D_0 D_1 p_{1,j}(T_0, T_1, T_2)$$
$$+ \frac{1}{\bar{M}_{jj}} \bar{f}_j \left( p_{0,1}(T_0, T_1, T), \ldots, p_{0,N}(T_0, T_1, T_2) \right) \tag{62}$$

in which $\bar{f}_i$  is a part of $f_i$ with third-order $\varepsilon$'s parameters:

$$\varepsilon^2 : D^2_0 p_{1,j}(T_0, T_1, T_1) + \omega^2_{0,j} p_{1,j}(T_0, T_1, T_1) = -2 D_0 D_1 p_{0,j}(T_0, T_1, T_2) \tag{63}$$

Consequently, the solution to Eq. (60) is:

$$p_{0,j}(T_0, T_1, T_1) = A_j(T_1, T_2) e^{i\omega_{0,j} T_0} + CC \tag{64}$$

where symbol $i$ represents the imaginary unit and CC corresponds to the complex conjugate of the preceding terms. The coefficients $A_j(T_1, T_2)$ of the unknown complex function can be determined by eliminating the secular terms given in the following paragraphs.

Now, substituting Eq. (64) into Eq. (61), the following equations are obtained:

$$\varepsilon^2 : D^2_0 p_{1,j}(T_0, T_1, T_1) + \omega^2_{0,j} p_{1,j}(T_0, T_1, T_1) = -2\left(i\omega_{0,j}\right) \frac{\partial A_j(T_1, T_2)}{\partial T_1} e^{i\omega_{0,j} T_0} + CC \tag{65}$$

Based on the secular terms of Eq. (65), one can write:

$$-2\left(i\omega_{0,j}\right) \frac{\partial A_j(T_1, T_2)}{\partial T_1} = 0 \rightarrow A_j(T_1, T_2) = \beta_j(T_2) \tag{66}$$

where $\beta_j(T_2)$ can be written (in polar form) as:

$$\beta_j(T_2) = \frac{1}{2} a_j(T_2) e^{i\phi_j(T_2)} \tag{67}$$

$$\bar{\beta}_j(T_2) = \frac{1}{2} a_j(T_2) e^{-i\phi_j(T_2)} \tag{68}$$

Substituting Eq. (67) into the following third-order approximate equation, we have:

$$\varepsilon^3 : D^2_0 p_{2,j}(T_0, T_1, T_1) + \omega^2_{0,j} p_{2,j}(T_0, T_1, T_1) = -2i\omega_{0,j} \frac{\partial \beta_j(T_2)}{\partial T_2} e^{i\omega_{0,j} T_0} + CC + \frac{1}{\bar{M}_{jj}} \bar{f}_j \left( p_{0,1}(T_0, T_1, T), \ldots, p_{0,N}(T_0, T_1, T_2) \right) + NSC \tag{69}$$

where NST denotes the non-secular terms. Now, substituting Eqs. (67) and (68) into Eq. (69), The following relations can be obtained:

**Table 1.** The positive real values of $\lambda_i$ for simply supported and clamped edge boundary conditions.

| Boundary conditions | $\lambda_1$ | $\lambda_2$ | $\lambda_3$ | $\lambda_4$ | $\lambda_5$ | $\lambda_6$ |
|---|---|---|---|---|---|---|
| Simply supported | 2.2215 | 5.4516 | 8.6114 | 11.7608 | 14.9068 | 18.0512 |
| Clamped edge | 3.1962 | 6.3064 | 9.4395 | 12.5771 | 15.7164 | 18.8565 |

**Table 2.** Comparison of dimensionless frequency parameter values $\Omega$ based on two different types of boundary conditions and classical plate theory ( $\Omega = \omega R^2 \sqrt{\rho h / D}$, $R = 10 nm$ ).

| Boundary conditions | $l$ (nm) | $\Omega_1$ | | $\Omega_2$ | |
|---|---|---|---|---|---|
| | | Ref. [69] | Present work | Ref. [69] | Present work |
| Simply supported | 0 | 4.9345 | 4.9350 | 29.7198 | 29.6961 |
| Clamped | 0 | 10.2158 | 10.2121 | 39.7706 | 39.6125 |
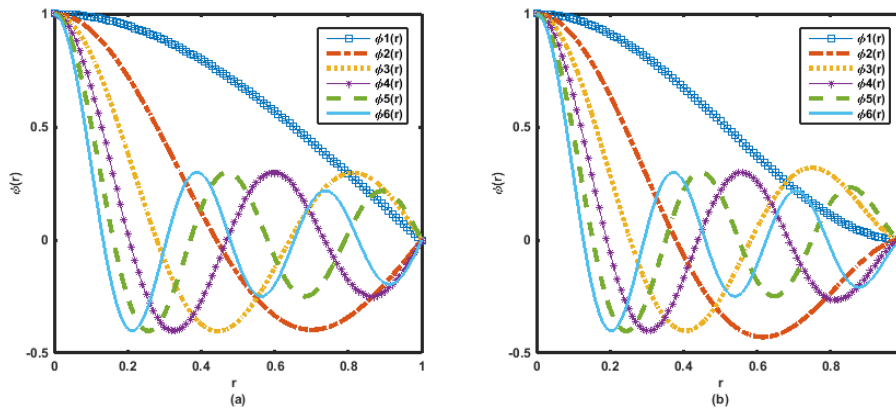


**Fig. 2.** Distribution of functions $\varphi_i(\overline{r})$ for (a) simply supported and, (b) clamped edge boundary conditions.

$$\varepsilon^3 : D^2_0 p_{2,j}(T_0,T_1,T_1) + \omega^2_{0,j} p_{2,j}(T_0,T_1,T_1) = -2i\omega_{0,j}\left(\frac{1}{2}\frac{\partial a_j(T_2)}{\partial T_2}e^{i\phi_j(T_2)} + \frac{1}{2}i\frac{\partial \phi_j(T_2)}{\partial T_2}a_i(T_2)e^{i\phi_j(T_2)}\right)e^{i\omega_{0,j}T_0} + CC$$
$$+ \frac{1}{\overline{M}_{jj}}\overline{f}_j\left(\frac{1}{2}a_1(T_2)e^{i\phi_1(T_2)}e^{i\omega_{0,1}T_0} + CC,...,\frac{1}{2}a_N(T_2)e^{i\phi_N(T_2)}e^{i\omega_{0,N}T_0} + CC\right) + NSC$$

(70)

As a result, based on the secular terms of Eq. (70), the secular expressions can be obtained as:

$$-2i\omega_{0,j}\left(\frac{1}{2}\frac{\partial a_i(T_2)}{\partial T_2}e^{i\phi_i(T_2)} + \frac{1}{2}i\frac{\partial \phi_i(T_2)}{\partial T_2}a_i(T_2)e^{i\phi_i(T_2)}\right) + \frac{1}{2\overline{M}_{jj}}\overline{f}_j\left(a_1(T_2),...,a_N(T_2),e^{i\phi_1(T_2)},e^{-i\phi_1(T_2)},...,e^{i\phi_N(T_2)},e^{-i\phi_N(T_2)}\right) = 0$$

(71)

Solving Eq. (71), $\phi_j$ and $a_j$ are obtained based on the fast time scale and initial conditions. Finally, based on Eqs. (67), (64), and (57), the expression $p_j(t,\varepsilon)$ is recast as:

$$p_j(\overline{t},\varepsilon) = a_j(T_2)\cos(\phi_j(T_2) + \omega_{0,j}T_0)$$

(72)

## 6. Numerical Results and Comparisons

In this study, the selected basic functions $\varphi_i(\overline{r})$ are used as the circular plate's linear free vibration mode shapes with the same boundary conditions to obtain the free vibrational solution of the nano-disk. Figure 2 shows the graphical representation of the mode functions, equations of which are given in (73):

$$\varphi_i(\overline{r}) = I_0(\lambda_i \overline{r}) - \frac{I_0(\lambda_i)}{J_0(\lambda_i)}J_0(\lambda_i \overline{r})$$

(73)

Here, $J_0$ and $I_0$ are the Bessel and modified Bessel functions of the first kind with the zeroth-order and positive real values for $\lambda_i$, presented in Table 1, for simply supported and clamped edges boundary conditions, utilized in this study (Leissa [67]; Leissa and Narita [68]).

To verify the accuracy of the present results, a comparison was made between the results given by (Mohammadi et al., [69]) and those from the current analysis for linear free vibrations of a classical circular plate ($l = 0$) in which the governing differential equations were solved utilizing the differential quadrature method (DQM) and similar boundary conditions. The first two non-dimensional frequencies are given in Table 2 for both types of boundary conditions. Good agreements are observed in the results for both types of boundary conditions. These results were deduced based on Young's modulus of $E = 1.06$ TPa, the mass density of $\rho = 2300$ kg/m$^3$, Poisson's ratio of $\nu = 0.3$, and a thickness of $h = 0.34$ nm.

**Table 3.** Comparison of the first three natural frequencies (kHz) for different thickness to length scale ratios of a circular microplate with $h = 100\mu m$.

| Boundary condition | Mode order | $\eta$ | l/h=0.1 | | l/h=0.5 | | l/h=1 | |
|---|---|---|---|---|---|---|---|---|
| | | | Present | Ref. [70] | Present | Ref. [70] | Present | Ref. [70] |
| Clamped | First Mode | 0.01 | 0.5614 | 0.5614 | 0.7658 | 0.7659 | 1.1977 | 1.1976 |
| | | 0.02 | 2.2455 | 2.2455 | 3.0632 | 3.0631 | 4.7903 | 4.7902 |
| | Second Mode | 0.01 | 2.1807 | 2.1854 | 2.9747 | 2.9811 | 4.6519 | 4.6620 |
| | | 0.02 | 8.7186 | 8.7380 | 11.8932 | 11.9196 | 18.5990 | 18.6403 |
| | Third Mode | 0.01 | 4.8953 | 4.8953 | 6.6777 | 6.6777 | 10.4428 | 10.4429 |
| | | 0.02 | 19.5600 | 19.5618 | 26.6819 | 26.6843 | 41,7263 | 41.7300 |
| Simply supported | First Mode | 0.01 | 0.2775 | 0.2775 | 0.3786 | 0.3786 | 0.5921 | 0.5921 |
| | | 0.02 | 1.1101 | 1.1101 | 1.5143 | 1.5143 | 2.3682 | 2.3681 |
| | Second Mode | 0.01 | 1.6381 | 1.6381 | 2.2331 | 2.2346 | 3.4923 | 3.4946 |
| | | 0.02 | 6.5458 | 6.5501 | 8.9292 | 8.9350 | 13.9638 | 13.9729 |
| | Third Mode | 0.01 | 4.0787 | 4.0789 | 5.5638 | 5.5641 | 8.7010 | 8.7013 |
| | | 0.02 | 16.3000 | 16.3005 | 22.2350 | 22.2355 | 34.7728 | 34.7728 |

**Table 4.** The effect of thickness to length scale ratio on the first dimensionless nonlinear frequency $\omega_{NL,1}$ for different dimensionless central vibration amplitudes in a circular micro-plate with $h/R$=0.01 and clamped boundary condition.

| $h/l$ | w(0,0)/h=0.2 | | w(0,0)/h=0.4 | | w(0,0)/h=0.6 | |
|---|---|---|---|---|---|---|
| | $\omega_{NL,1}$ | | $\omega_{NL,1}$ | | $\omega_{NL,1}$ | |
| | Ref. [51] | Present | Ref. [51] | Present | Ref. [51] | Present |
| Classical | 10.2931 | 10.3123 | 10.5240 | 10.6019 | 10.8970 | 11.0845 |
| 10 | 10.4808 | 10.4988 | 10.7065 | 10.7832 | 11.0730 | 11.2571 |
| 5 | 11.0220 | 11.0396 | 11.2381 | 11.3098 | 11.5871 | 11.7600 |
| 4 | 11.4109 | 11.4283 | 11.6195 | 11.6891 | 11.9587 | 12.1238 |
| 3 | 12.2109 | 12.2261 | 12.4052 | 12.4697 | 12.7234 | 12.8756 |
| 2 | 14.2481 | 14.2617 | 14.4155 | 14,4701 | 14.6894 | 14.8175 |
| 1 | 22.2310 | 22.2387 | 22.3373 | 22.3720 | 22.5150 | 22.5942 |

The present results are compared with those in Ref. [70] for further validations, based on the modified couple stress theory. Jomehzadeh et al. (Jomehzadeh et al., [70]) studied the free vibration analysis of a size-dependent circular micro-plate based on the modified couple stress theory. The micro-plates were assumed to be made of epoxy with the following material properties: ($E$ = 1.44 GPa, $\upsilon$ = 0.38, $\rho$ = 1220 Kg/m³ and $h/R$=0.01, and $h/R$=0.02). As shown in Table 3, good agreements are observed between the current findings and those in this reference.

In a relevant study, Wang et al. [51] used the modified couple stress theory to investigate the large amplitude free vibration of a size-dependent circular micro-plate. They employed the shooting method and the coding power of MATLAB to solve the governing equations. To verify the applicability and precision of the multi-scale method, the equations in this reference were solved again in the current study, utilizing the multi-scale method, based on the same parameters ($E$ = 1.44 GPa, $\upsilon$ = 0.38, $\rho$ = 1220 kg/m³, $h/R$=0.01, and $h = 100\ \mu m$), and the same initial and boundary conditions. As shown in Table 4, very good agreements are observed between the results of both methods. This indicates that the multi-scale method is useful, practical, and accurate and can be used for the solution of nano-structural problems.

In addition, Table 4 indicates that for a given value of the nonlocal parameter, the dimensionless frequency parameter increases with an increase in the dimensionless nonlocal parameter. Figure 3 depicts the vibrational transverse displacement of simply supported and clamped edge nano-disks for different non-dimensional nonlocal parameter, for the first mod and based on $w(0,0)/h$=1, $h/R$=0.01, and $\upsilon$ = 0.3. According to this figure, the natural frequency increases as the non-dimensional nonlocal parameter increases. Results from the classical von Kármán plate theory are also superimposed for further comparison. The difference between the transverse displacement predicted by the classical and non-classical models is clear for both types of boundary conditions. The difference in responses corresponding to similar values (of $l$) in both cases is more prominent at higher values of the nonlocal parameter $l$. As a result, one can conclude that the nonlocal parameter $l$ plays an important role in the determination of the transverse vibrational displacement of a nano-disk. Hence, to attain a correct solution, the application of nonlocal elasticity theory is mandatory.
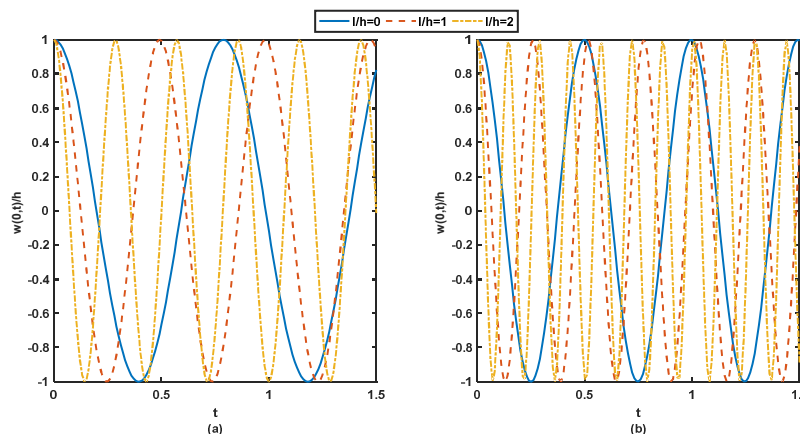


**Fig. 3.** Central dimensionless vibration displacements in a nano-disk for the different values of the nonlocal parameter, (a) simply supported boundary conditions, (b) clamped edge boundary conditions.
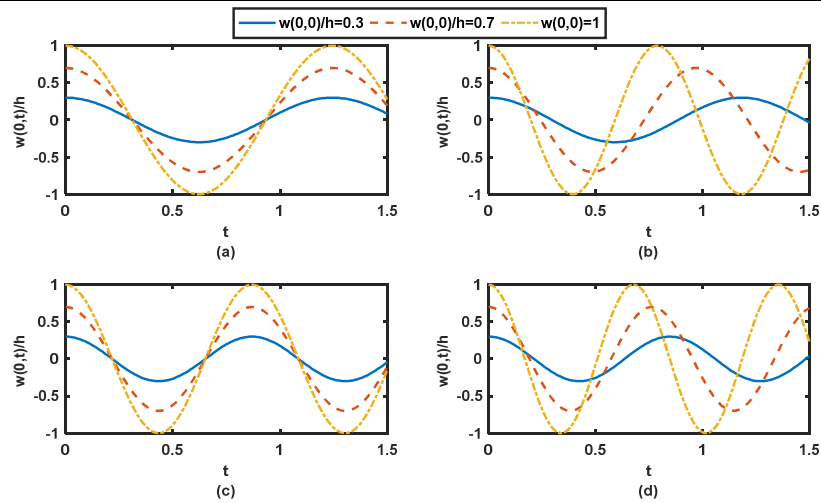
**Fig. 4.** Central dimensionless vibrational displacements of a nano-disk with the simply supported boundary conditions and $h/r$=0.01 at the different value of the initial central dimensionless amplitude, (a) linear, $l/h$=0, (b) nonlinear, $l/h$=0, (c) linear, $l/h$=0.5 and, (d) nonlinear, $l/h$=0.5.
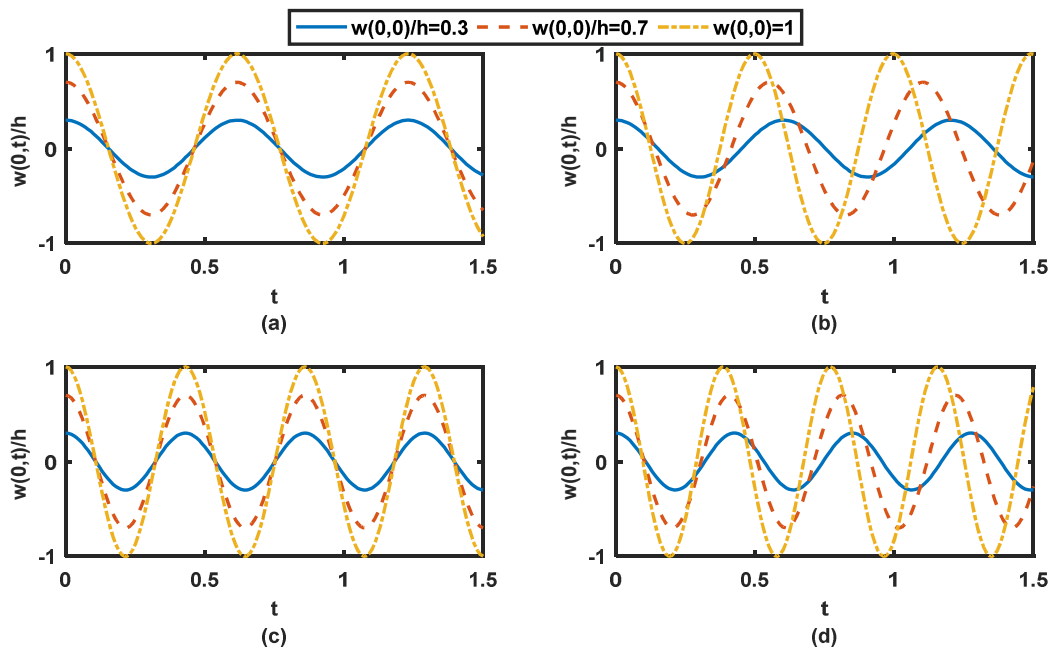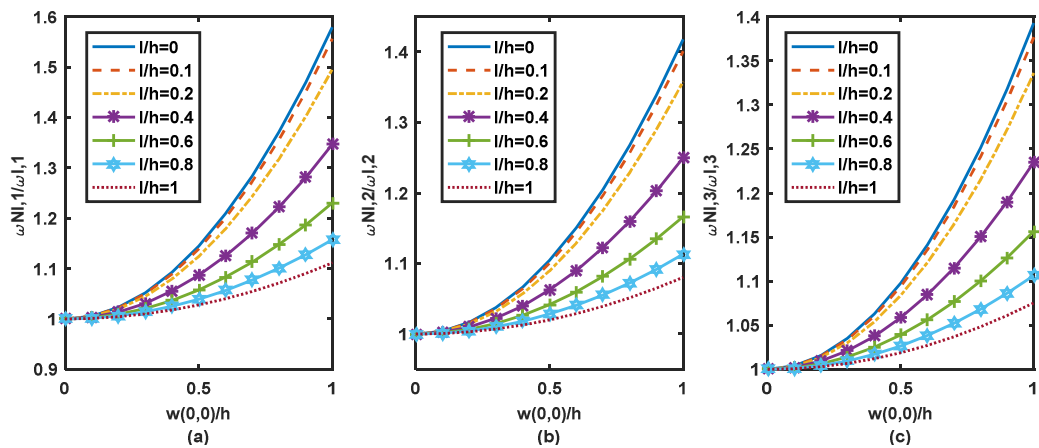


**Fig. 5.** Central dimensionless vibration displacements in a nano-disk with clamped edge boundary conditions and $h/r$=0.01 for the different values of the initial central dimensionless amplitude, (a) linear, $l/h$=0, (b) nonlinear, $l/h$=0, (c) linear, $l/h$=0.5 and, (d) nonlinear, $l/h$=0.5.



**Fig. 6.** Dependency of the nonlinear frequency ratios on the initial conditions, $w(0,0)/h$, for a simply supported nano-disk, (a) first mode, (b) second mode, and (c) third mode.
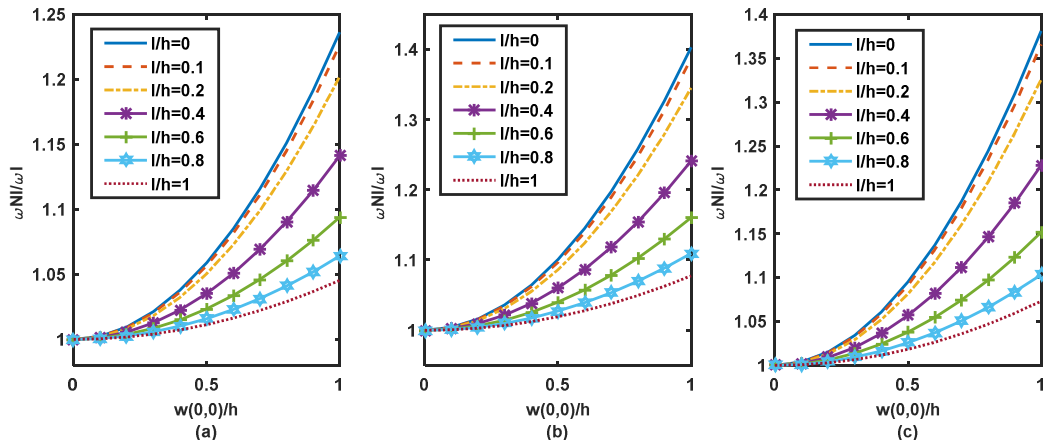
**Fig. 7.** Dependency of the nonlinear frequency ratios on the initial conditions, $w(0,0)/h$, for a clamped edge nano-disk, (a) first mode, (b) second mode, and (c) third mode.
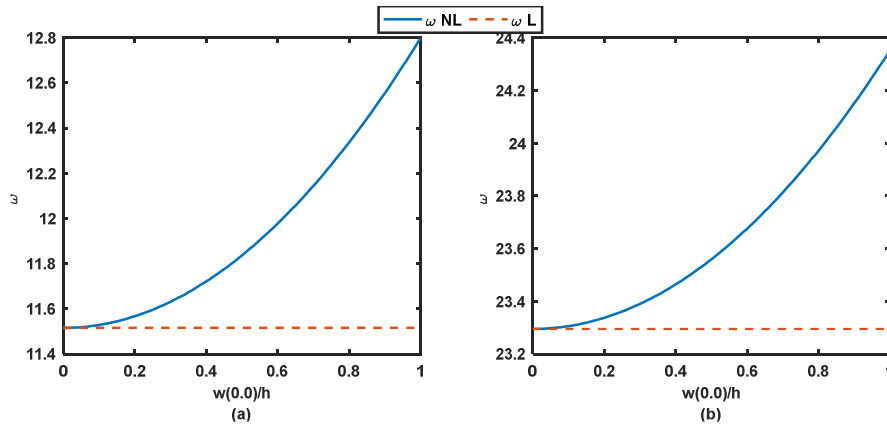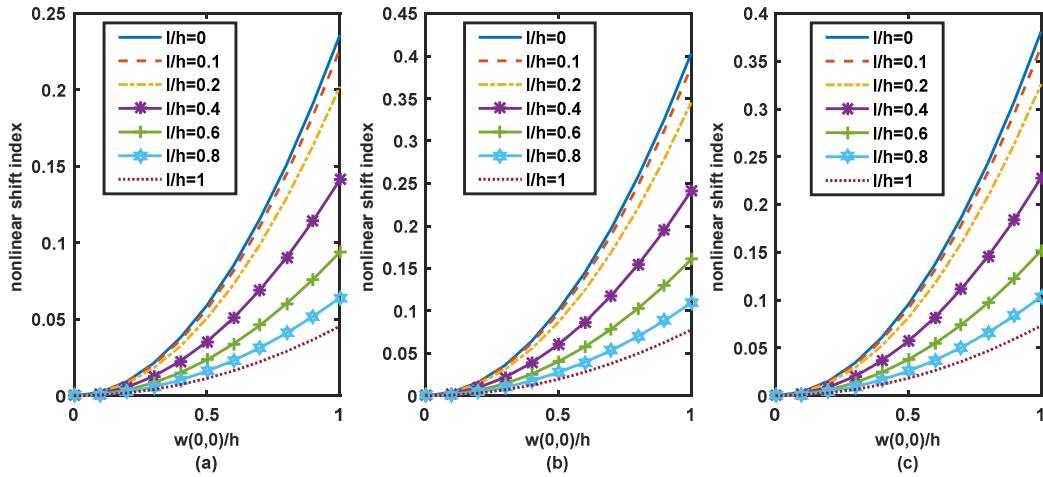


**Fig. 8.** The effect of dimensionless initial conditions of $w(0,0)/h$, on the linear and nonlinear natural frequencies based on $h/R=0.01$, $\nu = 0.3$ and $l/h=1$, (a) simply supported, and (b) clamped edge.
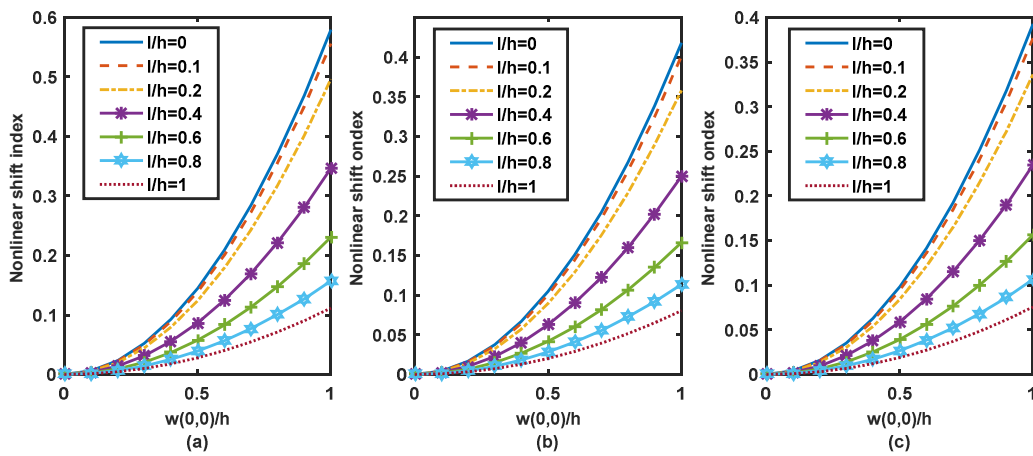


**Fig. 9.** Dependency of the nonlinear frequency ratios on the initial conditions, $w(0,0)/h$, for a clamped edge nano-disk, (a) first mode, (b) second mode, and (c) third mode.

**Fig. 10.** Dependency of the nonlinear shift index on the initial conditions $w(0,0)/h$, for a clamped edge nano-disk, (a) first mode, (b) second mode, and (c) third mode.
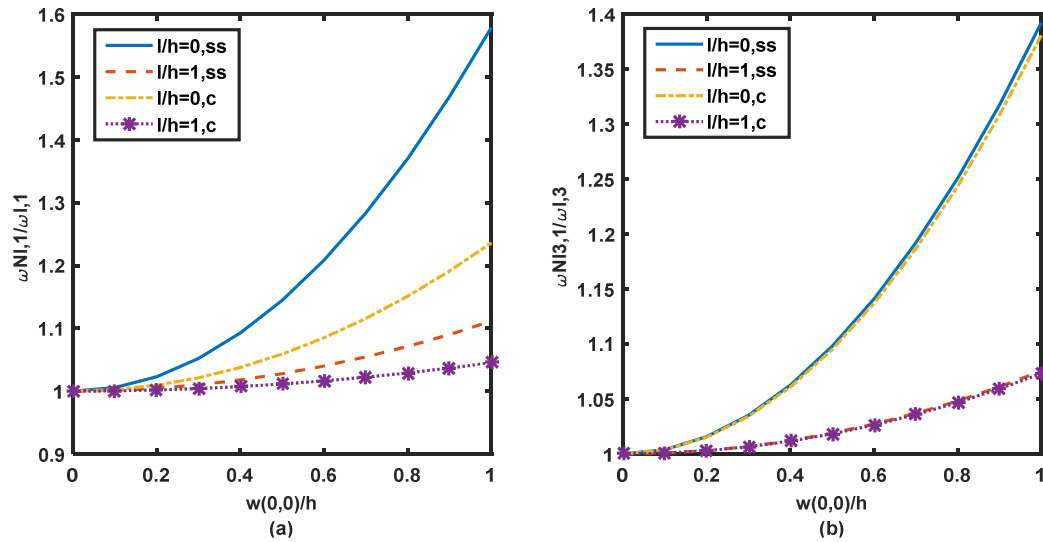


**Fig. 11.** The effect of support types on the nonlinear frequency ratios based on the classical ($l/h=0$) and non-classical theories ($l/h=1$), $h/r=0.01$, and $v = 0.3$, (a) first mode, and (b) third mode.
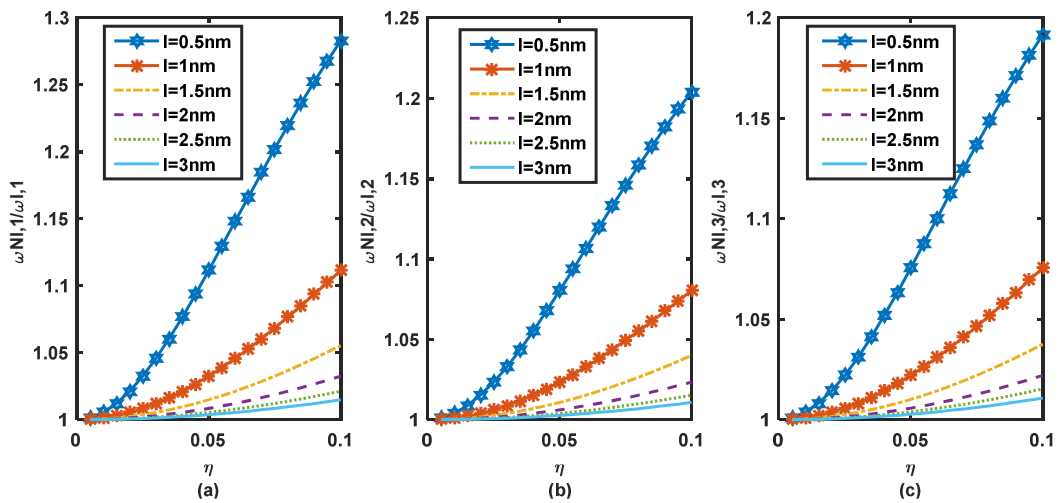


**Fig. 12.** Dependency of the nonlinear frequency ratios on $h/r$ for a simply supported nano-disk, (a) first mode, (b) second mode, and (c) third mode.

In addition, Figs. 4 and 5 demonstrate the vibrational transverse displacement of simply supported and clamped edge nano-

disks for various initial values of dimensionless central amplitude in the first mode. These figures are illustrated based on the geometric and mechanical properties of: $E = 1.06$ TPa, $\upsilon = 0.3$, $\rho = 2300$ Kg/m$^3$, and $R = 10$ nm. These figures reveal how some factors such as non-dimensional nonlocal parameters, dimensionless central amplitude, and the type of support could alter the vibration behavior of the circular nano-disk.

Figs. 6 and 7 illustrate the effects of non-dimensional nonlocal parameter $l/h$ on $\omega_{NI,i}/\omega_{l,i}$ (i=1,2,3), for different values of $w(0,0)/h$ and the two types of clamped edge and simply supported boundary conditions introduced before. These figures were generated based on the following geometric values and material properties; $E = 1.06$ TPa, $\upsilon = 0.3$, $\rho = 2300$ kg/m$^3$, $\eta = 0.01$ and $R = 10$ nm. Based on the results, the dimensionless frequency ratio of the nano-disc increases as the initial central dimensionless amplitude increases. This shows the dependency of the nonlinear frequency on the initial conditions (there is no such dependency in the linear models). To unveil this behavior, the linear and nonlinear natural frequencies of the nano-disk with the two types of clamped edge and simply supported boundary conditions with $h/R = 0.01$, $\upsilon = 0.3$, and $l/h = 1$, are shown in Figure 8. As is evident, $\omega_L$ is not dependent on dimensionless initial conditions, $w(0,0)/h$, while due to the nonlinear geometric properties from von Kármán plate theory, the dependency of $\omega_{NI,i}/\omega_{l,i}$ on the initial conditions is well observed. However, this ratio decreases as the non-dimensional nonlocal parameter increases. It is worth mentioning that for all values of the nonlocal parameter $l$, the vibrational frequencies predicted by the modified couple stress theory are greater than those by the classical theory. This indicates that the modified couple stress theory results in a stiffer plate compared with the classical plate theory.

For further investigations, Figs. 9 and 10 are plotted to show the effects of non-dimensional nonlocal parameter $l/h$ on the nonlinear shift index in the nano-disk frequency, for different values of $w(0,0)/h$, based on the clamped and simply supported boundary conditions. The nonlinear shift is an essential index in the nonlinear oscillation that is interpreted as the hardening or softening effect on the nano-disk motion. These figures are based on the geometric values and material properties introduced before.

Results indicate that the nonlinear shift in the nano-disk frequency increases as the initial central dimensionless amplitude increases. This important effect decreases as the non-dimensional nonlocal parameter increases. Accordingly, the hardening effect in the nano-disk vibrational behavior is observed for an increase in the initial central dimensionless amplitude or a decrease in the non-dimensional nonlocal parameter.
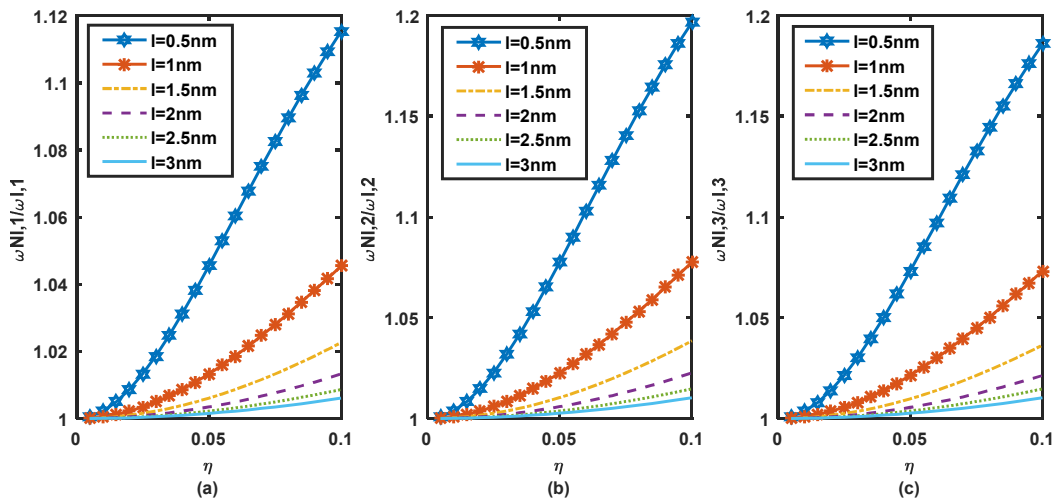


**Fig. 13.** Dependency of the nonlinear frequency ratios on $h/r$ for a clamped edge nano-disk, (a) first mode, (b) second mode, and (c) third mode.
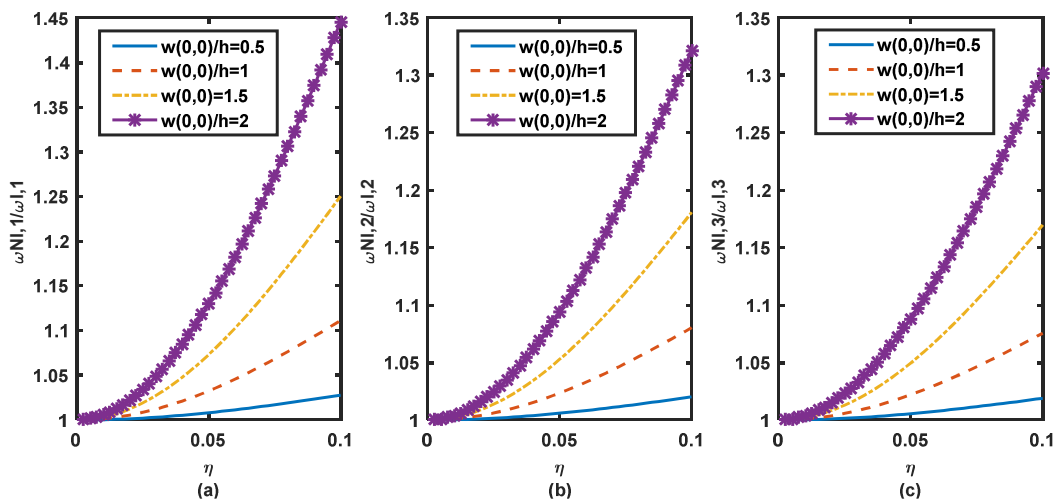


**Fig. 14.** The effect of $h/r$ on the nonlinear frequency ratio for a simply supported nano-disk, (a) first mode, (b) second mode, and (c) third mode.
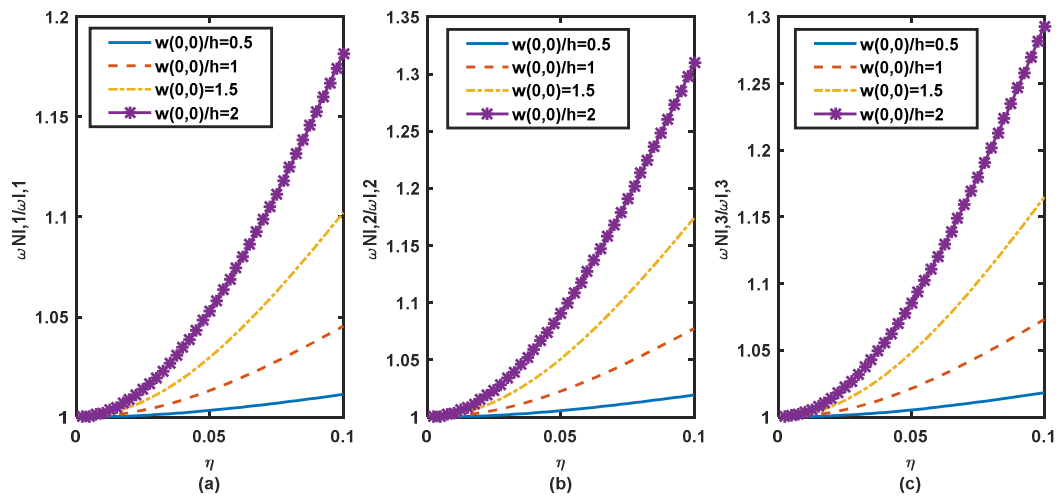
**Fig. 15.** The effect of $h/r$ on the nonlinear frequency ratio for a clamped edge nano-disk, (a) first mode, (b) second mode, and (c) third mode.

As the other alternative, Fig. 11 demonstrates the effect of supported type on $\omega_{Nl,i}/\omega_{l,i}$ (i=1, 3) ratio. As observed, this effect is more pronounced in classical theory ($l/h$=0), as well as lower mode numbers.

Figs. 12 and 13 illustrate the dependency of the nonlinear frequency ratios $\omega_{Nl,i}/\omega_{l,i}$ (i=1,2,3), on $\eta = h/r$, for different values of the nonlocal parameter and geometric and mechanical properties of ; $E$ =1.06 TPa, $\upsilon$ = 0.3, $\rho$ = 2300 Kg/m³, $R$=10 nm and $w(0,0)/h$ =1. It is observed that based on the modified couple stress theory, the ratio $\eta$ plays an important role in the nonlinear frequencies. Moreover, according to this theory, the effect of $\eta$ is more pronounced for lower values of the nonlocal parameter.

The nonlinear frequency ratios $\omega_{Nl,i}/\omega_{l,i}$ (i = 1,2,3) were plotted for three different values of initial conditions $w(0,0)/h$= 0.5, 1, 1.5 and 2 (Figs. 14 and 15), to study the effect of $\eta$ on the nano-disk transverse vibration. To extract these results, it was assumed that; $E$ = 1.06 TPa, $\rho$ = 2300 kg/m³, $\upsilon$ = 0.3, nonlocal parameter $l$ = 1 nm, and $R$ = 10 nm. It is observed that for the clamped and simply supported boundary conditions, the ratios of natural frequencies increase as the $h/R$ ratio increases. This increase is less prominent at lower initial values.

## 7.   Conclusions

In this study, the nonlinear free vibration analysis of a nano-disk was investigated using a modified couple stress model and von Kármán geometrically nonlinear theory. The model was size-dependent with a material length scale parameter $l$ to capture the size effect. The derived governing nonlinear equations were reduced to the classical von Kármán plate theory provided $l$ = 0. Using Hamilton's principle, the differential equations of motion were derived and the Galerkin weighted residual method in conjunction with the multi-scale method was used to solve the equations based on simply supported and clamped edge boundary conditions. Results indicate that the proposed method is precise and can be easily applied to extract the nonlinear characteristic relations for the frequency response of the nano-disks. It was also concluded that the nonlocal parameter $l_0$, central dimensionless amplitude, and the thickness to radius ratio $h/r$, play important roles in the vibrational behavior of the nano-disk. According to the results, it was found that for all values of the non-dimensional nonlocal parameter $l_0$, the linear and nonlinear natural frequencies predicted by the modified couple stress theory are greater than those based on the classical method. This indicates that the von Kármán plate model offers a stiffer plate compared to the modified couple stress theory. Additionally, the numerical results indicate that an increase in the central dimensionless amplitude leads to an increase in the nonlinear frequencies ratios and nonlinear shift index. Inversely, the increase in non-dimensional nonlocal parameter $l_0$ leads to a decrease in the nonlinear frequencies ratios and nonlinear shift index. This effect seems to be more conspicuous at lower vibrational modes. Examination of the results also indicates that for both types of boundary conditions used in this work, the differences in frequencies predicted by the classical and non-classical models are well noticeable at higher values of central dimensionless amplitude. Furthermore, according to the modified couple stress theory, the $h/r$ ratio has a significant impact on the nonlinear vibrational behavior of the nano-disk. Consequently, it can be concluded that increasing this ratio leads to an increase in the effect of dimensionless central amplitude on the nonlinear frequencies ratios of the nano-disk. This effect is more prominent at the lower values of $l_0$; meaning that the nonlocal effect can be only disregarded if the thickness-to-radius ratio, $h/r$, is highly insignificant. Furthermore, for each boundary condition used in this work, there is a difference in the transverse displacement predicted by the classical and non-classical models. This value is less prominent for higher values of the non-dimensional nonlocal parameters and higher vibrational modes. Moreover, the obtained results support the idea that the proposed MSM significantly reduces the computational effort and is a simple, reassuring, and yet highly effective method for dealing with many nonlinear problems that one might face in the field of mathematical physics.

## Authors' Contributions

All authors planned the scheme, initiated the project, developed the mathematical modeling, and examined the theory validation. The manuscript was written through the contribution of all authors. All authors discussed the results, reviewed, and approved the final version of the manuscript.

## Acknowledgments

## Conflict of Interest

## Funding

## Data Availability Statements

The datasets generated and/or analyzed during the current study are available from the corresponding author on reasonable request.

## References

[1] Tsai, N.-C., Liou, J.-S., Lin, C.-C., Li, T. Analysis and fabrication of reciprocal motors applied for microgyroscopes, *Journal of Micro/Nanolithography, MEMS, and MOEMS*, 8(4), 2009, 043046.

[2] Tsai, N.-C., Liou, J.-S., Lin, C.-C., Li, T. Design of micro-electromagnetic drive on reciprocally rotating disc used for micro-gyroscopes, *Sensors and Actuators A: Physical*, 157(1), 2010, 68-76.

[3] Tsai, N.-C., Liou, J.-S., Lin, C.-C., Li, T. Suppression of dynamic offset of electromagnetic drive module for micro-gyroscope, *Mechanical Systems and Signal Processing*, 25(2), 2011,680-693.

[4] Lee, S., Kim, D., Bryant, M.D., Ling, F.F. A micro corona motor, *Sensors and Actuators A: Physical*, 118(2), 2005, 226-232.

[5] Dolatabady, A., Granpayeh, N., Nezhad, V.F. A nanoscale refractive index sensor in two dimensional plasmonic waveguide with nanodisk resonator, *Optics Communications*, 300, 2013, 265-268.

[6] Zhang, Y., Tekobo, S., Tu, Y., Zhou, Q., Jin, X., Dergunov, S.A., et al. Permission to enter cell by shape: nanodisk vs nanosphere, *ACS applied materials & Interfaces*, 4(8), 2012, 4099-4105.

[7] Hwang, I., Choi, J., Hong, S., Kim, J.-S., Byun, I.-S., Bahng, J.H., et al. Direct investigation on conducting nanofilaments in single-crystalline Ni/NiO core/shell nanodisk arrays, *Applied Physics Letters*, 96(5), 2010, 053112.

[8] Horejs, C., Pum, D., Sleytr, U.B., Peterlik, H., Jungbauer, A., Tscheliessnig, R. Surface layer protein characterization by small angle X-ray scattering and a fractal mean force concept: from protein structure to nanodisk assemblies, *The Journal of Chemical Physics*, 133(17), 2010, 11B602.

[9] Hägglund, C., Zäch, M., Petersson, G., Kasemo, B. Electromagnetic coupling of light into a silicon solar cell by nanodisk plasmons, *Applied Physics Letters*, 92(5), 2008, 053110.

[10] Huang, C.-H., Igarashi, M., Horita, S., Takeguchi, M., Uraoka, Y., Fuyuki, T., et al. Novel Si nanodisk fabricated by biotemplate and defect-free neutral beam etching for solar cell application, *Japanese Journal of Applied Physics*, 49(4S), 2010, 04DL16.

[11] Ito, T., Audi, A.A., Dible, G.P. Electrochemical characterization of recessed nanodisk-array electrodes prepared from track-etched membranes, *Analytical Chemistry*, 78(19), 2006, 7048-7053.

[12] Ito, T., Perera, D.-M., editors, Electrochemical studies of recessed nanodisk-array electrodes prepared from track-etched membranes, *Meeting Abstracts*, 2007.

[13] Luo, L., White, H.S. Electrogeneration of single nanobubbles at sub-50-nm-radius platinum nanodisk electrodes, *Langmuir*, 29(35), 2013, 11169-11175.

[14] Chin, M.K., Chu, D.Y., Ho, S.T. Estimation of the spontaneous emission factor for microdisk lasers via the approximation of whispering gallery modes, *Journal of Applied Physics*, 75(7), 1994, 3302-3307.

[15] Cao, H., Xu, J., Xiang, W., Ma, Y., Chang, S.-H., Ho, S., et al. Optically pumped InAs quantum dot microdisk lasers, *Applied Physics Letters*, 76(24), 2000, 3519-3521.

[16] Van Campenhout, J., Rojo-Romeo, P., Regreny, P., Seassal, C., Van Thourhout, D., Verstuyft, S., et al. Electrically pumped in P-based microdisk lasers integrated with a nanophotonic silicon-on-insulator waveguide circuit, *Optics Express*, 15(11), 2007, 6744-6749.

[17] Kwon, S.-H., Kang, J.-H., Kim, S.-K., Park, H.-G. Surface plasmonic nanodisk/nanopan lasers, *IEEE Journal of Quantum Electronics*, 47(10), 2011, 1346-1353.

[18] Cho, S.-Y., Jokerst, N.M. A polymer microdisk photonic sensor integrated onto silicon, *IEEE Photonics Technology Letters*, 18(20), 2006, 2096-2098.

[19] Aifantis, E.C. *Strain gradient interpretation of size effects*, Fracture Scaling: Springer; 1999, 299-314.

[20] Anjomshoa, A., Tahani, M. Vibration analysis of orthotropic circular and elliptical nano-plates embedded in elastic medium based on nonlocal Mindlin plate theory and using Galerkin method, *Journal of Mechanical Science and Technology*, 30(6), 2016, 2463-2474.

[21] Sedighi, H.M., Size-dependent dynamic pull-in instability of vibrating electrically actuated microbeams based on the strain gradient elasticity theory, *Acta Astronautica*, 95, 2014, 111-123.

[22] Koochi, A., H.M. Sedighi, and M. Abadyan, Modeling the size dependent pull-in instability of beam-type NEMS using strain gradient theory, *Latin American Journal of Solids and Structures*, 11, 2014, 1806-1829.

[23] Mindlin, R.D., Eshel, N. On first strain-gradient theories in linear elasticity, *International Journal of Solids and Structures*, 4(1), 1968, 109-124.

[24] Toupin, R. Elastic materials with couple-stresses, *Archive for Rational Mechanics and Analysis*, 11(1), 1962, 385-414.

[25] Yang, F., Chong, A., Lam, D.C.C., Tong, P. Couple stress based strain gradient theory for elasticity, *International Journal of Solids and Structures*, 39(10), 2002, 2731-2743.

[26] Eringen, A.C. Nonlocal polar elastic continua, *International Journal of Engineering Science*, 10(1), 1972, 1-16.

[27] Eringen, A.C. On differential equations of nonlocal elasticity and solutions of screw dislocation and surface waves, *Journal of Applied Physics*, 54(9), 1983, 4703-4710.

[28] Eringen, A. Nonlocal continuum field theories: *Springer Science & Business Media*, 2002.

[29] Shishesaz, M., Shariati, M., Yaghootian, A. and Alizadeh, A., Nonlinear Vibration Analysis of Nano-Disks Based on Nonlocal Elasticity Theory Using Homotopy Perturbation Method, *International Journal of Applied Mechanics,* 11(02), 2019, 1950011.

[30] Shishesaz, M., Shariati, M., Yaghootian, A., Nonlocal Elasticity Effect on Linear Vibration of Nano-circular Plate Using Adomian Decomposition Method, *Journal of Applied and Computational Mechanics*, 6(1), 2020, 63-76.

[31] Barretta, R. and F.M. de Sciarra, Analogies between nonlocal and local Bernoulli–Euler nanobeams, *Archive of Applied Mechanics*, 85(1), 2015, 89-99.

[32] Demir, C., et al., Bending response of nanobeams resting on elastic foundation, *Journal of Applied and Computational Mechanics*, 4(2), 2018, 105-114.

[33] Malikan, M., On the buckling response of axially pressurized nanotubes based on a novel nonlocal beam theory, *Journal of Applied and Computational Mechanics*, 5(1), 2019, 103-112.

[34] Chen, J., Tian, Y., Cui, X. Free and forced vibration analysis of peridynamic finite bar, *International Journal of Applied Mechanics*, ,10(01), 2018, 1850003.

[35] Diyaroglu, C., Oterkus, E., Oterkus, S., Madenci, E. Peridynamics for bending of beams and plates with transverse shear deformation, *International Journal of Solids and Structures*, 69, 2015, 152-168.

[36] O'Grady, J., Foster, J. Peridynamic plates and flat shells: A non-ordinary, state-based model, *International Journal of Solids and Structures*, 51(25-26), 2014, 4572-4579.

[37] Barretta, R., et al., Nonlocal inflected nano-beams: A stress-driven approach of bi-Helmholtz type, *Composite Structures*, 200, 2018, 239-245.

[38] Barretta, R., et al., A stress-driven local-nonlocal mixture model for Timoshenko nano-beams, *Composites Part B: Engineering*, 164, 2019, 590-598.

[39] Barretta, R., M. Canadija, and F.M. de Sciarra, On thermomechanics of multilayered beams, *International Journal of Engineering Science*, 155, 2020, 103364.

[40] Romano, G., R. Barretta, and M. Diaco, Iterative methods for nonlocal elasticity problems, *Continuum Mechanics and Thermodynamics*, 31(3), 2019, 669-689.

[41] Apuzzo, A., et al., Axial and torsional free vibrations of elastic nano-beams by stress-driven two-phase elasticity, *Journal of Applied and*

*Computational Mechanics*, 5(2), 2019, 402-413.

[42] Miandoab, E.M., Pishkenari, H.N., Yousefi-Koma, A., Hoorzad, H. Polysilicon nano-beam model based on modified couple stress and Eringen's nonlocal elasticity theories, *Physica E: Low-dimensional Systems and Nanostructures*, 63, 2014, 223-228.

[43] Asghari, M., Kahrobaiyan, M., Rahaeifard, M., Ahmadian, M. Investigation of the size effects in Timoshenko beams based on the couple stress theory, *Archive of Applied Mechanics*, 81(7), 2011, 863-874.

[44] Liu, D., Chen, W. Size-dependent thermomechanical responses of nano-sized multilayers, *Journal of Nanomechanics and Micromechanics*, 5(1), 2015, A4014003.

[45] Baghani, M. Analytical study on size-dependent static pull-in voltage of microcantilevers using the modified couple stress theory, *International Journal of Engineering Science*, 54, 2012, 99-105.

[46] Akgöz, B., Civalek, Ö. Thermo-mechanical buckling behavior of functionally graded microbeams embedded in elastic medium, *International Journal of Engineering Science*, 85, 2014, 90-104.

[47] Pal, S., Das, D. Free Vibration Behavior of Rotating Bidirectional Functionally-Graded Micro-Disk for Flexural and Torsional Modes in Thermal Environment, *International Journal of Mechanical Sciences*, 2020, 105635.

[48] Shaat, M., Mahmoud, F., Gao, X.-L., Faheem, A.F. Size-dependent bending analysis of Kirchhoff nano-plates based on a modified couple-stress theory including surface effects, *International Journal of Mechanical Sciences*, 79, 2014, 31-37.

[49] Veysi, A., Shabani, R., Rezazadeh, G. Nonlinear vibrations of micro-doubly curved shallow shells based on the modified couple stress theory, *Nonlinear Dynamics*, 87(3), 2017, 2051-2065.

[50] Jouneghani, F.Z., Dashtaki, P.M., Dimitri, R., Bacciocchi, M., Tornabene, F. First-order shear deformation theory for orthotropic doubly-curved shells based on a modified couple stress elasticity, *Aerospace Science and Technology*, 73, 2018, 129-147.

[51] Wang, Y.-G., Lin, W.-H., Liu, N. Large amplitude free vibration of size-dependent circular microplates based on the modified couple stress theory, *International Journal of Mechanical Sciences*, 71, 2013, 51-57.

[52] Karamanli, A., Aydogdu, M. Free vibration and buckling analysis of laminated composites and sandwich microbeams using a transverse shear-normal deformable beam theory, *Journal of Vibration and Control*, 26(3-4), 2020, 214-228.

[53] Ghadiri, M., Shafiei, N. Vibration analysis of rotating functionally graded Timoshenko microbeam based on modified couple stress theory under different temperature distributions, *Acta Astronautica*, 121, 2016, 221-240.

[54] Ghadiri, M., SafarPour, H. Free vibration analysis of size-dependent functionally graded porous cylindrical microshells in thermal environment, *Journal of Thermal Stresses*, 40(1), 2017, 55-71.

[55] Malikan, M., Buckling analysis of a micro composite plate with nano coating based on the modified couple stress theory, *Journal of Applied and Computational Mechanics*, 4(1), 2018, 1-15.

[56] Jomehzadeh, E., Saidi, A. Study of small scale effect on nonlinear vibration of nano-plates, *Journal of Computational and Theoretical Nanoscience*, 9(6), 2012, 864-871.

[57] He, X., Wang, J., Liu, B., Liew, K. M. Analysis of nonlinear forced vibration of multi-layered graphene sheets, *Computational Materials Science*, 61, 2012, 194-199.

[58] Zhang, L., Zhang, Y., Liew, K. Modeling of nonlinear vibration of graphene sheets using a meshfree method based on nonlocal elasticity theory, *Applied Mathematical Modelling*, 49, 2017, 691-704.

[59] Foda, M.A. Influence of shear deformation and rotary inertia on nonlinear free vibration of a beam with pinned ends, *Computers & Structures*, 71(6), 1999, 663-670.

[60] Ramezani, A., Alasty, A., Akbari, J. Effects of rotary inertia and shear deformation on nonlinear free vibration of microbeams, *Journal of Vibration and Acoustics*, 128(5), 2006, 611-615.

[61] El-Dib, Y., Stability analysis of a strongly displacement time-delayed Duffing oscillator using multiple scales homotopy perturbation method, *Journal of Applied and Computational Mechanics*, 4(4), 2018, 260-274.

[62] Romano, G., R. Barretta, and M. Diaco, Micromorphic continua: non-redundant formulations, *Continuum Mechanics and Thermodynamics*, 28(6), 2016, 1659-1670.

[63] Barbagallo, G., et al., Transparent anisotropy for the relaxed micromorphic model: macroscopic consistency conditions and long wave length asymptotics, *International Journal of Solids and Structures*, 120, 2017, 7-30.

[64] Neff, P., et al., Real wave propagation in the isotropic-relaxed micromorphic model, *Proceedings of the Royal Society A: Mathematical, Physical and Engineering Sciences*, 473(2197), 2017, 20160790.

[65] Faris, W.F., *Nonlinear dynamics of annular and circular plates under thermal and electrical loadings*, Virginia Tech, 2003

[66] Nayfeh, A.H., Mook, D.T. *Nonlinear oscillations*, John Wiley & Sons, 2008.

[67] Leissa, A.W. *Vibration of plates*, Scientific and Technical Information Division, National Aeronautics and Space Administration, 1969.

[68] Leissa, A., Narita, Y. Natural frequencies of simply supported circular plates, *Journal of Sound and Vibration*, 70(2), 1980, 221-229.

[69] Mohammadi, M., Ghayour, M., Farajpour, A. Free transverse vibration analysis of circular and annular graphene sheets with various boundary conditions using the nonlocal continuum plate model, *Composites Part B: Engineering*, 45(1), 2013, 32-42.

[70] Jomehzadeh E, Noori H and Saidi A. The size-dependent vibration analysis of micro-plates based on a modified couple stress theory, *Physica E*, 43(4), 2011, 877-883.

## ORCID iD

Ali Alizadeh  https://orcid.org/0000-0003-2275-7365
Mohammad Shishesaz  https://orcid.org/0000-0002-1892-1946
Shahram Shahrooi  https://orcid.org/0000-0003-3367-6712
Arash Reza  https://orcid.org/0000-0003-0320-5434

**Publisher's Note** Shahid Chamran University of Ahvaz remains neutral with regard to jurisdictional claims in published maps and institutional affiliations.